Journal of Applied Polymer Science

WILEY

Applied Polymer SCIENCE

RESEARCH ARTICLE OPEN ACCESS

Flame Retardant Performance of Phosphatized Starch in Epoxy Resins: A Sustainable Approach to Enhancing Fire Safety

Florian Rothenhäusler[1] | Felix Ludik[1] | Lena Geiling[2] | Holger Ruckdaeschel[1]

[1]Department of Polymer Engineering, University of Bayreuth, Bayreuth, Germany | [2]Chair of Electrochemical Process Engineering, University of Bayreuth, Bayreuth, Germany

Correspondence: Holger Ruckdaeschel (holger.ruckdaeschel@uni-bayreuth.de)

Received: 29 January 2025 | **Revised:** 21 March 2025 | **Accepted:** 27 March 2025

Funding: This work was supported by the German Federal Ministry for Economic Affairs and Climate Action (BMWK) within the research projects "EcoPrepregs-Grundlagenforschung zur Klärung der Struktur-Eigenschaftsbeziehungen von Epoxidharzen und Fasern aus nachwachsenden Rohstoffen zur Anwendung in der Sekundärstruktur von Flugzeugen" (grant # 20E1907A, Germany) and "NewPreg-Nachhaltige, wirtschaftliche und funktionalisierte Bio-Feststoffharz-Prepregtechnologie zur CO_2-Reduktion durch kühlfreie Lagerung, Einsatz erneuerbarer Ressourcen und Gewichtsreduktion durch maßgeschneidertes Drapierverhalten" (grant # 20Q2227C, Germany).

Keywords: bio-based | epoxy resin | flame retardant | phosphatized starch | sustainability

ABSTRACT

The imperative to protect human life and property from the threat of fires underscores the need for effective flame retardants (FRs). In response to growing calls for sustainability, bio-based FR options have emerged, among which phosphatized starch (PS) has shown considerable promise. This study investigates the FR mechanisms and FR performance of thermally stabilized PS in epoxy resin-based thermosets through thermo-gravimetric analysis, thermo-gravimetric Fourier-transform infrared spectroscopy mass spectrometry, and cone calorimetry. PS primarily acts in the condensed phase by promoting the formation of char and an intumescent layer. Incorporating 25% of PS into the thermoset significantly reduces the peak heat release rate, total heat release, and total smoke release by 70%, 52%, and 53%, respectively. As the global pursuit of responsible and environmentally conscious fire safety solutions intensifies, exploring PS as a bio-based FR represents a promising step toward a safer and more sustainable future.

1 | Introduction

Flame retardants (FRs) are important means to protect human life and property from the dangers of fires [1–3]. Among the potential alternatives for halogenated FR [4–6], phosphorus-based FRs have emerged as a promising solution to address these concerns [7, 8]. They are renowned for their capacity to effectively hinder combustion by encouraging the formation of char, which acts as a protective, intumescent barrier, thus halting the spread of flames [9]. Moreover, they may disrupt the radical chain reaction in the flame zone through phosphorus-containing radicals generated during combustion [10]. Additionally, they yield significantly fewer toxic byproducts than halogenated FRs when exposed to fire, rendering them a safer choice for fire safety applications [11]. However, commercial phosphorus-based FRs are currently largely derived from non-renewable feedstocks, which is why interest in the development of bio-based, phosphorous FRs has increased in light of growing environmental and sustainability concerns [12, 13]. Bio-based FRs are sourced from renewable materials, reducing our dependence on non-renewable resources and lowering carbon emissions.

Within this sustainable framework, phosphatized starch (PS) has emerged as a strong contender among bio-based FRs [14, 15]. Starch, derived from plants, is abundant and easily accessible, making it an ideal starting material for sustainable FR

[Correction added on 2 March 2026, after first online publication: The copyright line was changed.]

development [16]. PS is typically synthesized by blending urea and phosphatizing agents with starch and allowing the mixture to react at temperatures around 135°C for several hours (see Figure 1) [17]. This process transforms the starch's anhydroglucose units (AGU) into various esters, including phosphate, ammonium phosphate, and carbamate groups, depending on the reaction conditions [17, 18]. Despite being utilized as an FR for wood fibers, expandable polystyrene foams, paper, and cotton, PS has not been widely applied to polymeric bulk materials, primarily due to its limited thermal stability [19–25]. However, a previous investigation by the authors has addressed this issue by modifying the synthesis route of PS, improving its thermal stability via thermal modification that removes residual urea and thermally unstable carbamate groups, and promoting the formation of ammonium polyphosphate groups before polymer processing [26].

This paper delves into the FR performance of PS as a bio-based FR for epoxy resin-based thermosets, marking the pioneering use of PS as FR in a polymeric bulk material. Through utilizing techniques such as thermo-gravimetric analysis (TGA), thermo-gravimetric Fourier-transform infrared spectroscopy mass spectrometry (TG-FTIR-MS), and cone calorimetry (CC), the FR mechanisms and flame retardancy of PS are evaluated.

2 | Experimental

2.1 | Materials

The resin system uses diglycidyl ether of bisphenol A (DGEBA) (epoxide equivalent weight of 187 g/mol) from Blue Cube Assets GmbH & Co. KG, Olin Epoxy (Stade, Germany) as resin in combination with dicyandiamide in the form of DYHARD100S from Alzchem Group AG (Trostberg, Germany) as curing agent. The curing reaction is accelerated by an urea-based accelerator, called DYHARDUR500, from Alzchem Group AG.

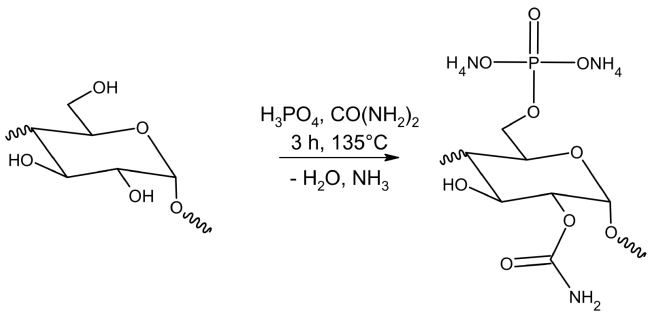

FIGURE 1 | Synthesis of PS using urea and phosphoric acid.

The PS was synthesized according to the procedure utilized by the authors in a previous study [26], which modified the synthesis route by Heinze et al. [17] by adding a thermal modification step. The thermal modification enables the processing of PS at elevated temperatures necessary for thermoset curing by reducing the risk of pore formation. The phosphorus content of the PS was about 15.9%.

2.2 | Resin Formulation

The resin mixtures were weighed in according to their respective composition as detailed in Table 1. The mass ratio of DGEBA to dicyandiamide was kept constant for all thermosets. The accelerator was added so that it is 1% of DGEBA plus dicyandiamide. PS was added in 5% from 0% to 25%. The mixtures were mixed using a centrifuge speed mixer from Hauschild Engineering (Hamm, Germany) at 3000 min^{-1} for 120 s. To ensure the removal of any trapped air prior to curing, the mixtures were degassed for 30 min at 10 mbar.

2.3 | Curing Cycle and Sample Preparation

The mixtures were cured in aluminum molds for 2 h at 135°C within a Memmert UF55plus oven from Memmert GmbH + Co. KG (Schwabach, Germany). Following the curing process, the molds were gradually cooled to room temperature over a 4-h duration. Specimens for testing were then prepared from the cured plates in accordance with the relevant ISO standards for each test method. These specimens were created using a Mutronic DIADISC5200 diamond plate saw and a Mutronic Diadrive 2000 from MUTRONIC Präzisionsgerätebau GmbH & Co. KG (Rieden am Forggensee, Germany).

2.4 | Material Characterization

2.4.1 | Thermo-Gravimetric Analysis

The TGA were performed using a Netzsch 209 F1 Libra instrument from Erich Netzsch GmbH & Co. Holding KG (Selb, Germany). The thermosets were heated from 30°C to 1000°C at

TABLE 1 | Compositions of the thermosets.

Label	DGEBA in %	Dicyandiamide in %	PS in %	DYHARDUR500 in %
PS0	93	6.0	0	1
PS5	88.35	5.7	5	0.95
PS10	83.7	5.4	10	0.9
PS15	79.05	5.1	15	0.85
PS20	74.4	4.8	20	0.8
PS25	69.75	4.5	25	0.75

a constant rate of $10\,^{\circ}\mathrm{C}/\,\mathrm{min}$ under nitrogen or synthetic air. The flow rate of both gases was set to 30 mL/min. Samples weighing about 15 mg were tested in triplicate.

2.4.2 | Thermo-Gravimetric Fourier-Transform Infrared Spectroscopy Mass Spectrometry

TG-FTIR-MS was performed by combining a STA 449 C Jupiter from Erich Netzsch GmbH & Co. Holding KG (Selb, Germany) with a VERTEX 70v FTIR spectrometer from Bruker (Billerica, Massachusetts, US) and a QMS 403 AëolosQuadro from Erich Netzsch GmbH & Co. Holding KG (Selb, Germany). Samples weighing approximately 15 mg were subjected to heating from 30°C to 1000°C at a constant rate of $10\,^{\circ}\mathrm{C}/\,\mathrm{min}$ under nitrogen or synthetic air. The flow rate of both gases was set to 45 mL/min. The transport lines to the FTIR and MS instruments were kept at 230°C. Volatile degradation products were analyzed every 17 s by averaging 32 scans over a wavenumber range from 600 to 4000 cm^{-1} in transmission mode.

To enhance comparability, the TG-MS ion currents were normalized to a sample mass of exactly 15 mg. For better clarity, the TG-FTIR spectra were normalized to the largest signal at the respective temperature. It has to be kept in mind that this might also make smaller signals appear larger, especially if the concentration of volatile compounds analyzed is low. It is imperative to acknowledge a certain temporal discrepancy between the initiation of thermoset decomposition, the liberation of low molecular weight compounds leading to weight loss as detected by TGA, and the subsequent detection of these volatile compounds via FTIR and MS after the conveyance through the transport lines. Therefore, TG-FTIR and TG-MS data typically lag by a few seconds behind the TGA data.

2.4.3 | Cone Calorimetry

The assessment of the fire behavior of the thermosets and FR performance of the PS was conducted using CC in accordance with ISO 5660-1 [27]. A Fire Testing Technology "iCone" device (East Grinstead, UK) was employed for the experiments. The specimens, weighing about 40 g and measuring 100 mm by 100 mm by 3 mm, were subjected to a heat flux of $35\ \mathrm{kW}/\mathrm{m}^2$ with the heating coil positioned 25 mm away. Consistent with the methodologies of Perret et al. and Neumeyer et al. the tests continued until the smoke release rate reached a constant and negligible level for 15 s [28, 29].

Calculating the Flame Retardancy Index (FRI) provides another perspective on evaluating the effectiveness of FR formulations compared to the neat epoxy thermoset [30, 31]. The product of the total heat release (THR) and the peak heat release rate (PHRR) divided by the time to ignition (TTI) of the neat matrix material, that is, the epoxide thermoset, is normalized to the corresponding product of the FR formulations:

$$\mathrm{FRI} = \frac{\left(\mathrm{THR}\cdot\frac{\mathrm{PHRR}}{\mathrm{TTI}}\right)_{\mathrm{Ref}}}{\left(\mathrm{THR}\cdot\frac{\mathrm{PHRR}}{\mathrm{TTI}}\right)_{\mathrm{x}}} \tag{1}$$

It becomes evident that effective flame retardancy, according to this definition, is present when the FRI > 1. According to Vahabi et al. materials with an FRI between 1 and 10 are considered good, while FRI > 10 are classified as excellent [32]. Furthermore, CC enables the quantitative evaluation of individual FR mechanisms and their impact on the flame retardancy of various FR systems [33, 34]. These mechanisms include gas phase-based mechanisms, such as flame inhibition and fuel dilution (FIFD), as well as condensed phase-based mechanisms, such as charring and the protective layer effect (PLE) [35]. FIFD influence the effective heat of combustion (EHC), allowing the effect of both gas-phase mechanisms to be calculated as:

$$\Delta_{\mathrm{FIFD}} = \left(1 - \frac{\mathrm{EHC_x}}{\mathrm{EHC_{Ref}}}\right)\cdot 100\,\% \tag{2}$$

using the EHC of the FR sample $\mathrm{EHC_x}$ and the EHC of the reference $\mathrm{EHC_{Ref}}$.

Charring in the condensed phase results in a reduction in the released fuel and can be determined from the mass loss of the FR sample $\mathrm{ML_x}$ and the reference $\mathrm{ML_{Ref}}$:

$$\Delta_{\mathrm{Charring}} = \left(1 - \frac{\mathrm{ML_x}}{\mathrm{ML_{Ref}}}\right)\cdot 100\,\%\,. \tag{3}$$

The identified parameters for FIFD and charring describe the reduction in the respective key properties relative to the reference [36]. Similarly, the influence of intumescence through the PLE can be determined by considering the PHRR and the total heat evolved (THE) of the FR sample and the reference:

$$\Delta_{\mathrm{PLE}} = \left(1 - \frac{\mathrm{PHRR_x}\quad \mathrm{THE_{Ref}}}{\mathrm{PHRR_{Ref}}\quad \mathrm{THE_x}}\right)\cdot 100\,\%\,. \tag{4}$$

It is important to emphasize that Δ_{PLE} in this mathematical formulation does not represent the reduction of a specific property. In contrast, Δ_{FIFD} and $\Delta_{\mathrm{Charring}}$ quantify the percentage reduction in the EHC and ML, respectively. Due to the division of the PHRR ratio by the THE ratio, Δ_{PLE} can yield counterintuitive values, such as negative values, or strong variations in both directions with increasing FR weight fractions [36]. Ideally, a mathematical approach aimed at expressing the influence of intumescence on the reduction of CC properties should exhibit a more stable trend in its resulting coefficient. As part of the methodological innovation in this work, we propose the thermal protection index (TPI), which is closely related to the FRI and Δ_{PLE}. The TPI quantifies the effect of protective layers on the reduction of PHRR and THR:

$$\mathrm{TPI} = \frac{(\mathrm{THR}\cdot\mathrm{PHRR})_{\mathrm{Ref}}}{(\mathrm{THR}\cdot\mathrm{PHRR})_{\mathrm{x}}}. \tag{5}$$

Effective protection by intumescent layers is indicated when the TPI is greater than 1. The higher the TPI, the greater the influence of intumescence in the FR specimens. While Equation (5) can be applied to any two sets of CC results, the calculated TPI is only meaningful if intumescence is verified as the primary mode of FR action. The practical utility of this new index will be demonstrated in Section 3.2.

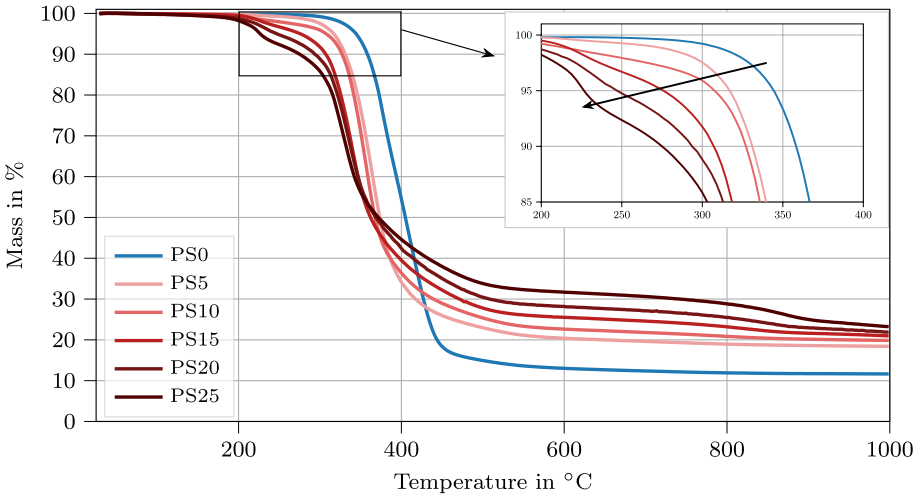

FIGURE 2 | TGA thermograms of thermosets with different weight fractions of PS under nitrogen. [Color figure can be viewed at wileyonlinelibrary.com]

2.4.4 | Scanning Electron Microscopy

The surfaces of CC specimens were examined using a Zeiss Gemini 1530 Scanning Electron Microscope from Carl Zeiss AG (Oberkochen, Germany). The analysis was carried out with an acceleration voltage of 3 kV, and the surfaces were coated with a layer of platinum sputtering, with a thickness of approximately 5 nm for enhanced imaging.

3 | Results and Discussion

3.1 | Thermo-Gravimetric Analysis and Thermo-Gravimetric Fourier-Transform Infrared Spectroscopy Mass Spectrometry

The following discussion delves into the thermal stability, thermal decomposition mechanisms, and FR mechanisms of PS in DGEBA-type thermosets. This requires the simultaneous analysis of TGA, TG-FTIR, and TG-MS data under both nitrogen and synthetic air. Special emphasis is placed on the TG-FTIR-MS data of PS0 and PS25, as these represent the most extreme cases in terms of their composition: no PS added and the maximum weight fraction of PS investigated.

First, the TGA thermograms and TG-FTIR-MS data of thermosets with different weight fractions of PS under nitrogen are analyzed. The main decomposition of PS0 takes place in a single step, starting at around 300°C, resulting in a mass loss of approximately 85% (see Figure 2). This is followed by a gradual mass loss at around 450°C, leaving 10.9% of residual mass at 1000°C. The TG-FTIR data of PS0 under nitrogen at temperatures between 325°C and 950°C (see Figure 3) reveals that in the beginning water (3400 4000 cm^{-1} and 1300 1800 cm^{-1}) and amines (3250 cm^{-1}) are released [37, 38]. The corresponding TG-MS data shows that the ion currents of ammonia or OH radicals ($m/z = 17$), and water ($m/z = 18$) increase slightly at the onset of decomposition (see Figure 4). The amines might result from the decomposition of the thermoset network itself or from the decomposition of residual dicyandiamide in the epoxy matrix [39–41].

Resulting from the main decomposition step, distinct signals in the TG-FTIR-MS data evidence the presence of DGEBA decomposition products which indicate the decomposition of the thermoset network [42]. At 750 and 3650 cm^{-1}, sharp signals emerge which signify the presence of phenolic compounds: methyl phenol ($m/z = 108$), and ethyl phenol or isopropyl phenol ($m/z = 122$) [43]. The aromatic ring structures of decomposition products of DGEBA are evidenced by peaks at 1600 and 1510 cm^{-1} (mainly CC & CCH), as well as 1260 and 1180 cm^{-1} (mainly CO & COH) [44]. The corresponding TG-MS data shows a drastic increase in the ion currents of benzene ($m/z = 78$), toluene ($m/z = 92$), phenol ($m/z = 94$) and methyl phenol ($m/z = 108$) [45, 46]. Other characteristic bands evidence the release of carbonyl compounds (1730 cm^{-1}) [47]. Subsequently, the aromatic structures break down into CH_3 radicals ($m/z = 15$) and CO_2 ($m/z = 44$). The TG-FTIR signals for CO_2 are evidenced by characteristic peaks at 670, 2310 and 2380 cm^{-1}. The CH_2 and CH_3 groups of the aromatic rings and their decomposition products form several peaks in between 2875 and 3100 cm^{-1} [48]. Notably, there is a sharp peak at 3015 cm^{-1}, signaling the release of methane [43].

During the final decomposition step, two peaks (2110 and 2180 cm^{-1}) indicating the release of CO become more pronounced. Since the mass loss rate is minimal during the final decomposition step, the TG-FTIR-MS signals of aromatic compounds decrease significantly. Notably, the ion current of CO_2 shows a double peak. The first is related to the initial decomposition of the thermoset network, while the second most likely results from the decomposition of larger aromatic compounds [49].

After elucidating the TG-FTIR-MS data of PS0, it is essential to analyze the influence of PS on the thermal decomposition mechanisms and thermal stability of DGEBA cured with dicyandiamide. Increasing the weight fraction of PS in the thermoset leads to a decreased decomposition temperature, as evidenced by the decreased temperatures at which 5% ($T_{5\%}$) and 10% mass loss ($T_{10\%}$) are recorded (see Figure 5). Two effects come into play: first, the PS itself has a significantly lower thermal stability than the epoxy matrix [26]. PS undergoes glycosidic bond cleavage (GBC) at temperatures

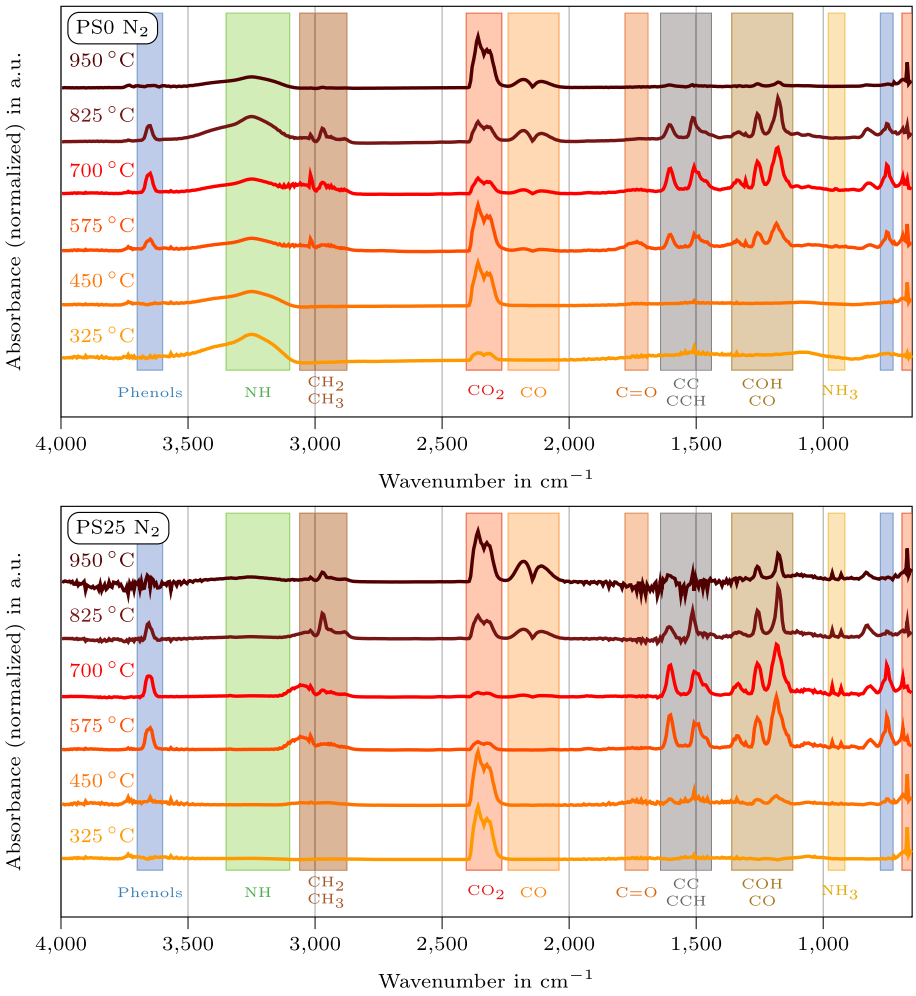

FIGURE 3 | The TG-FTIR data of PS0 and PS25 at temperatures between 325°C and 950°C under nitrogen. [Color figure can be viewed at wileyonlinelibrary.com]

as low as 180°C, leading to a significant mass loss and the release of ammonia, water and CO_2 [22, 26, 50]. Second, the ammonium phosphate groups release phosphoric acid which causes an acid catalyzed decomposition of the epoxy matrix [34, 51].

This is most pronounced for PS25, which shows an additional decomposition step beginning at around 185°C, coinciding with the GBC of PS. The TG-FTIR-MS data of PS25 under nitrogen at temperatures between 325°C and 950°C (see Figure 3) shows that water and CO_2 are released at the beginning. In contrast to the TG-FTIR spectra of PS0, no significant signals for amines appear at the start of PS25 decomposition. Apart from the emergence of two peaks at 930 and 965 cm^{-1}, indicating the release of ammonia, the FTIR spectra of PS0 and PS25 are qualitatively identical [52]. The ammonia most likely results from condensation reactions between neighboring ammonium phosphate groups, forming new P—O—P bonds [53, 54]. This process was postulated by Camino et al. who observed the release of ammonia and water in a 2:1 M ratio during the decomposition of ammonium polyphosphate [55]. In line with the decreased decomposition temperature of PS25 compared to that of PS0, the TG-FTIR signals corresponding to the breakdown of the thermoset network reach their maxima at lower temperatures. This is also evidenced by the TG-MS data which shows that the ion currents peak at lower temperatures for PS25 than for PS0.

The mass loss resulting from the main decomposition step of the thermoset decreases significantly for higher weight fractions of PS. Figure 5 shows that the mass at 600°C increases from 12.3% for PS0 to 31.7% for PS25. Notably, this value is much higher than the 21.5% predicted by a linear rule of mixture for PS25. Consequently, the incorporation of PS into DGEBA-type thermosets results in synergistic effects in terms of char formation at elevated temperatures.

The reason for the increased mass is the dehydration and esterification reactions caused by phosphoric acid released from the PS [19, 56, 57]. The subsequent cross-linking and aromatization of the char limit the release of flammable gases and lead to higher residual masses [58]. Accordingly, the ion current of CH_3 radicals shows only comparatively small increases. Levchik et al. demonstrated that phosphorous FRs improve flame retardancy of DGEBA-type thermosets by delaying the decomposition and release of DGEBA fragments. The DGEBA decomposition products are volatile and significantly contribute to feeding the flame [59].

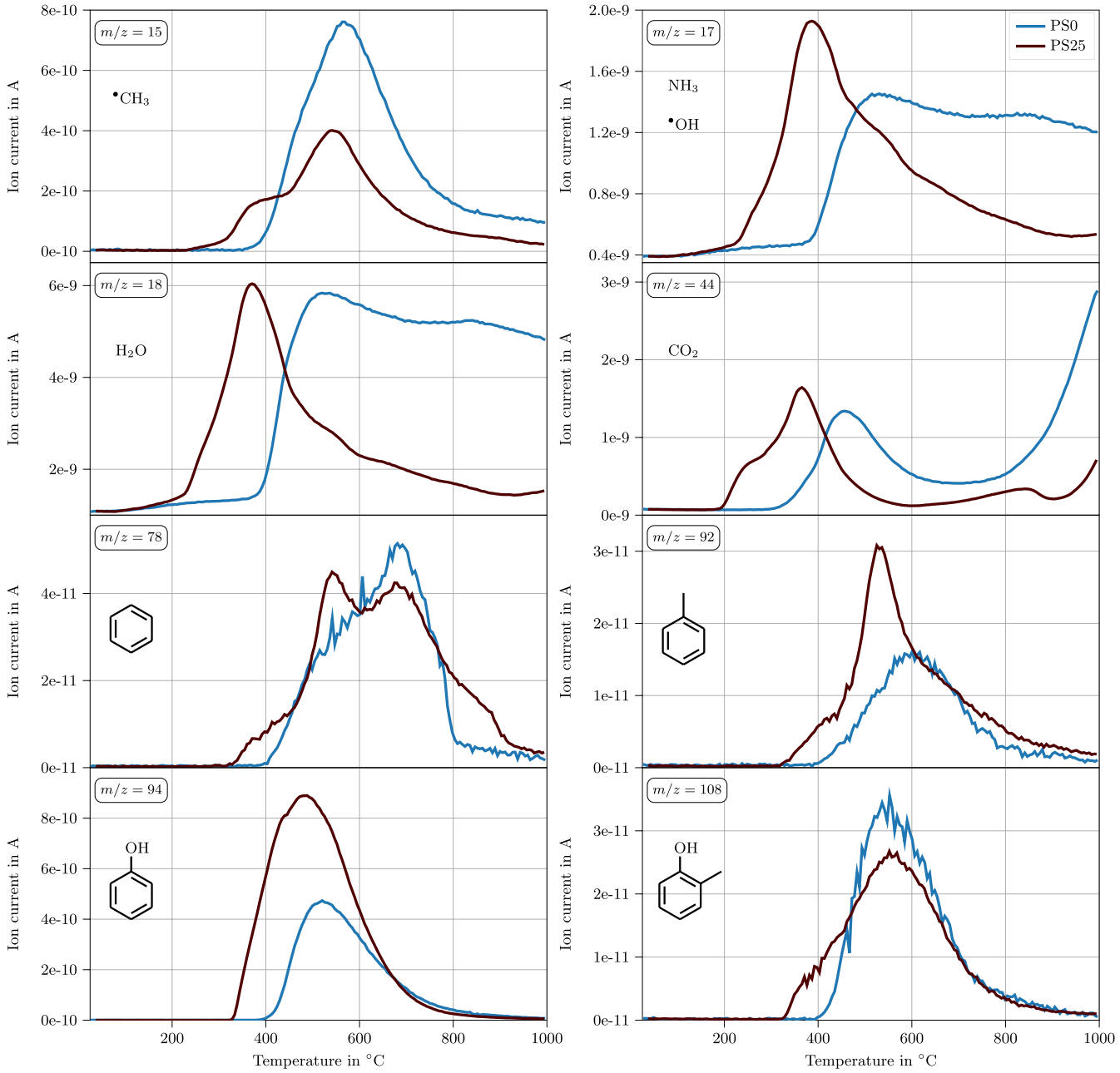

FIGURE 4 | The TG-MS data of PS0 and PS25 under nitrogen. [Color figure can be viewed at wileyonlinelibrary.com]

Furthermore, with increasing PS weight fraction, an additional, albeit small, mass loss between roughly 800°C and 900°C can be observed. Rothenhäusler et al. noted a steep mass loss in TG-FTIR at around the same temperature while investigating the thermal decomposition of PS and attributed it to the decomposition of phosphate groups and subsequent release of PO-type compounds [26]. Elemental analysis of chars after pyrolysis in the TGA showed that the phosphorus content decreased from 19.2% to 4.4% in this temperature range.

Still, detecting the presence of PO-type species resulting from the decomposition of PS in DGEBA-type matrices is difficult for several reasons. First, the phosphorus in the ammonium phosphate groups is fully oxidized, making it active in the condensed phase rather than in the gas phase [8, 43]. This leads to the increased masses after the main decomposition step. Second, the wavenumber at which characteristic signals are usually found ($P{=}O$ at approximately 1250 cm^{-1}) overlap with signals resulting from the decomposition of the epoxy matrix [60]. Third, the mass loss between 800°C and 900°C is comparatively small, resulting in low signal intensity.

After elucidating the thermal stability, thermal decomposition mechanisms, and FR mechanisms of PS in DGEBA-type thermosets under nitrogen, the discussion continues with the analysis of these mechanisms under synthetic air. Similar to the previously conducted analyses, this discussion will begin with a focus on the TG-FTIR-MS data of PS0 and then switch to PS25. In contrast to the TGA thermogram under nitrogen, PS0 decomposes in a two-step process under synthetic air (see Figure 6).

While the onset of decomposition under synthetic air is similar to that under nitrogen, the initial mass loss is significantly reduced (85% vs. 70%). Therefore, the decomposition of the thermoset network in the presence of oxygen leads to different decomposition mechanisms and products. The second decomposition step starts around 450°C, reducing the mass to 1% at around 680°C.

The TG-FTIR-MS data of PS0 under synthetic air differs drastically compared to that under nitrogen (see Figures 7 and 8). Water and amines are released at the beginning of the main decomposition, and there are no signals for amines and only low signals for hydrocarbons during the first decomposition step. The low molecular hydrocarbons are quickly oxidized, resulting in large signals for CO_2. The TG-MS data shows similar findings, in which the ion current of CH_3 radicals increases only marginally compared to that under nitrogen. Similarly, the signals corresponding to the aromatic decomposition products are greatly diminished but still present in the TG-FTIR spectra.

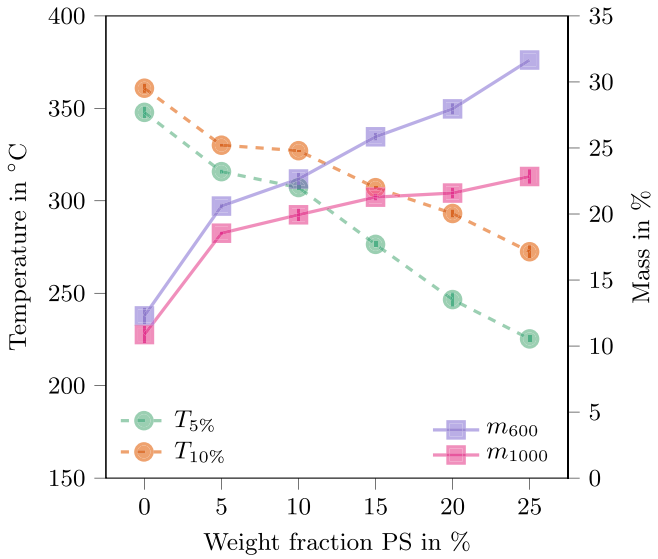

FIGURE 5 | $T_{5\%}$, $T_{10\%}$, m_{600} and m_{1000} of thermosets with different weight fractions of PS under nitrogen. [Color figure can be viewed at wileyonlinelibrary.com]

Similar to the trends observed in the TGA thermograms for the addition of PS into the thermosets, the decomposition temperature decreases for increased weight fractions of PS under synthetic air. Again, this leads to an additional decomposition step at around 185°C. During the main decomposition step, the reactions of the PS in the condensed phase reduce the mass loss. This effect is most notable during the final stages of decomposition, where the temperature at which the residual mass reaches its final value increases significantly with higher weight fractions of PS. For instance, PS0 exhibits 10% mass at 580°C, whereas PS25 shows 33.2% at the same temperature. Conversely, PS25 reaches 10% mass at around 750°C, indicating a notable delay in thermo-oxidative decomposition of the char. After the last decomposition step, approximately 1.8% of residual mass remains for PS25. Previous investigations have attributed this phenomenon to the formation of polyphosphate-based inorganic glasses [50, 61].

Figure 7 illustrates that the TG-FTIR signals corresponding to hydrocarbons, phenols and aromatic structures are significantly increased for PS25 compared to PS0 due to the delayed decomposition of release of DGEBA fragments [59]. In contrast to the TG-FTIR spectra of PS25 under nitrogen, the corresponding spectra under synthetic air show minimal peaks at 930 and 965 cm^{-1}, indicating the reduced presence of ammonia in the evolved gases. Similar to the TG-MS data under nitrogen, the ion current of CH_3 radicals of PS25 under synthetic air starts to increase at lower temperatures but reaches a lower maximum value compared to that of PS0. The additional decomposition step that occurs with the addition of PS into the thermoset at the onset of its decomposition is also indicated by increased ion currents of ammonia and OH radicals, and water. Naturally, the ion current of CO_2 is significantly increased under synthetic air compared to that under nitrogen (compare Figures 4 and 8). While the ion current of CO_2 of PS0 shows only one maximum, the ion current of PS25 displays several maxima, indicating the GBC of PS, the first and second decomposition steps of the matrix, and the breakdown and oxidation of larger aromatic

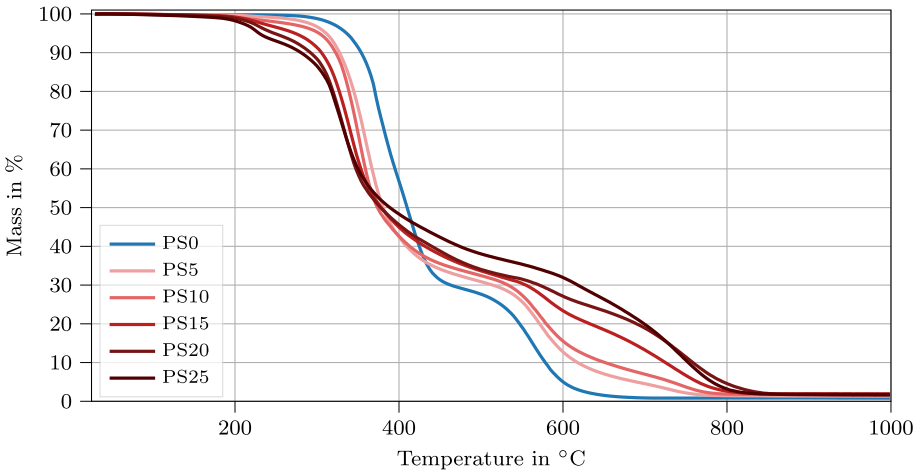

FIGURE 6 | TGA thermograms of thermosets with different weight fractions of PS under synthetic air. [Color figure can be viewed at wileyonlinelibrary.com]

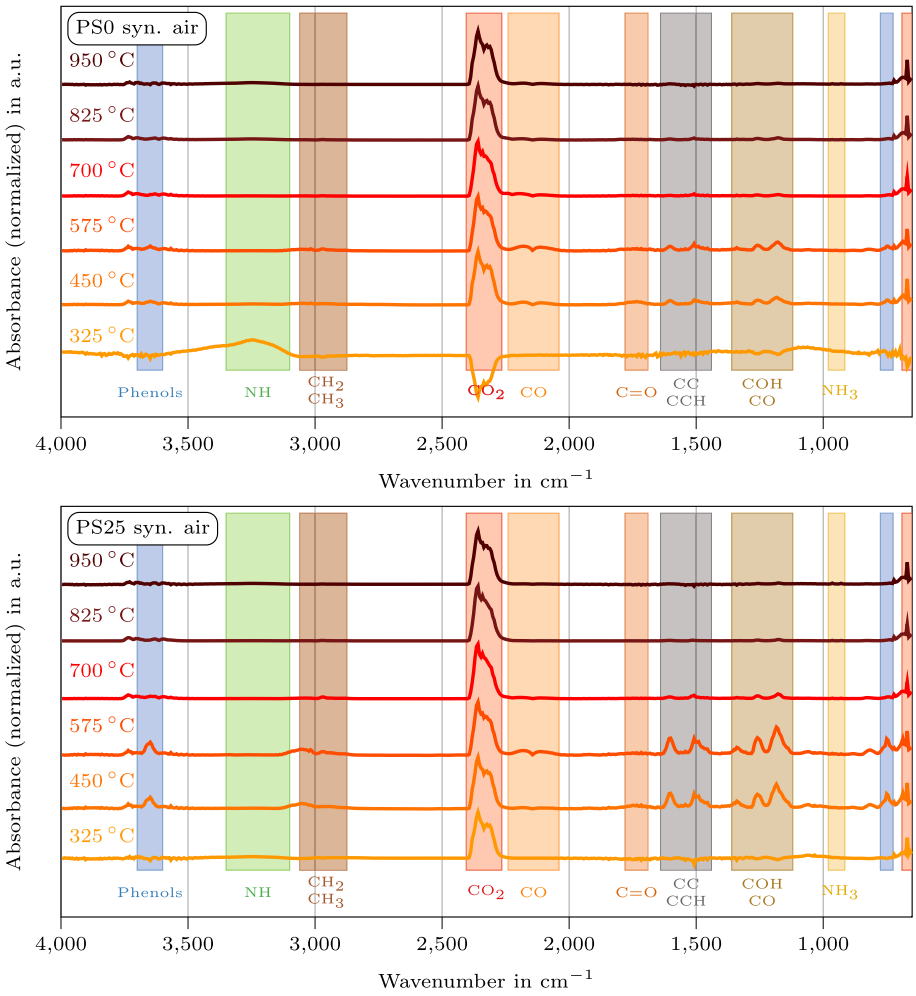

FIGURE 7 | The TG-FTIR data of PS0 and PS25 at temperatures between 325°C and 950°C under synthetic air. [Color figure can be viewed at wileyonlinelibrary.com]

molecules, respectively. The last two maxima of CO_2 of PS25 are notably delayed, demonstrating the stabilization effect of the PS in the condensed phase [59].

3.2 | Cone Calorimetry

The FR performance of PS and the fire behavior of the thermosets are evaluated using CC (see Figure 9). As expected from the TGA results, PS0 exhibits the longest TTI at 77 s. The HRR peaks shortly after at about 819 kW/m^2, leading to nearly complete incineration of the specimens. This results in a THR of about 91.6 MJ/m^2 and an ML of approximately 90.6%. Consequently, the smoke release rate (SRR) and thus the total smoke release (TSR) of PS0 are comparatively high (2866 m^2/m^2). In this process, the maximum average rate of heat emission (MARHE) reaches about 345 kW/m^2. For aerospace, railway and marine applications, high heat releases and smoke productions pose significant hazards to both the vehicle and its passengers.

However, with the addition of 5% PS, the PHRR of PS5 decreases to 483 kW/m^2, while the TTI is reduced to 61 s. This reduction is attributed to the actions of PS in the condensed phase, which cause the acid-catalyzed decomposition of the thermoset network, promote char formation and stabilization [9, 10]. This is accompanied by a noticeable increase in the expansion exhibited by the CC specimens during testing. Previous studies on PS as FR in lignocellulosic materials have demonstrated that PS is a strong intumescent agent [19, 22]. Intumescence describes a charred layer that shields the intact matrix material beneath it from the heat of the flame while simultaneously slowing down the transfer of pyrolysis products into the flame zone [62, 63]. Consequently, the THR and TSR are reduced to 69.1 and 2190 m^2/m^2, respectively. Likewise, the MAHRE is significantly lowered to roughly 260 kW/m^2.

As the weight fraction of PS increases further in the thermoset, the TTI, PHRR, MARHE, THR, and TSR continue to decrease significantly (see Figure 10). However, the incremental effects of each subsequent addition of 5% of PS become smaller. At the highest weight fraction of PS in the thermoset (PS25), ignition occurs at about 45 s and the HRR peaks shortly after at 244 kW/m^2. The initial burning of the material triggers the FR mechanisms, causing the HRR to decrease to about 150 kW/m^2 for a span of 120 s, during which the material burns slowly and forms an intumescent char layer [64]. In this process, the starch backbone of PS likely acts as a carbonization

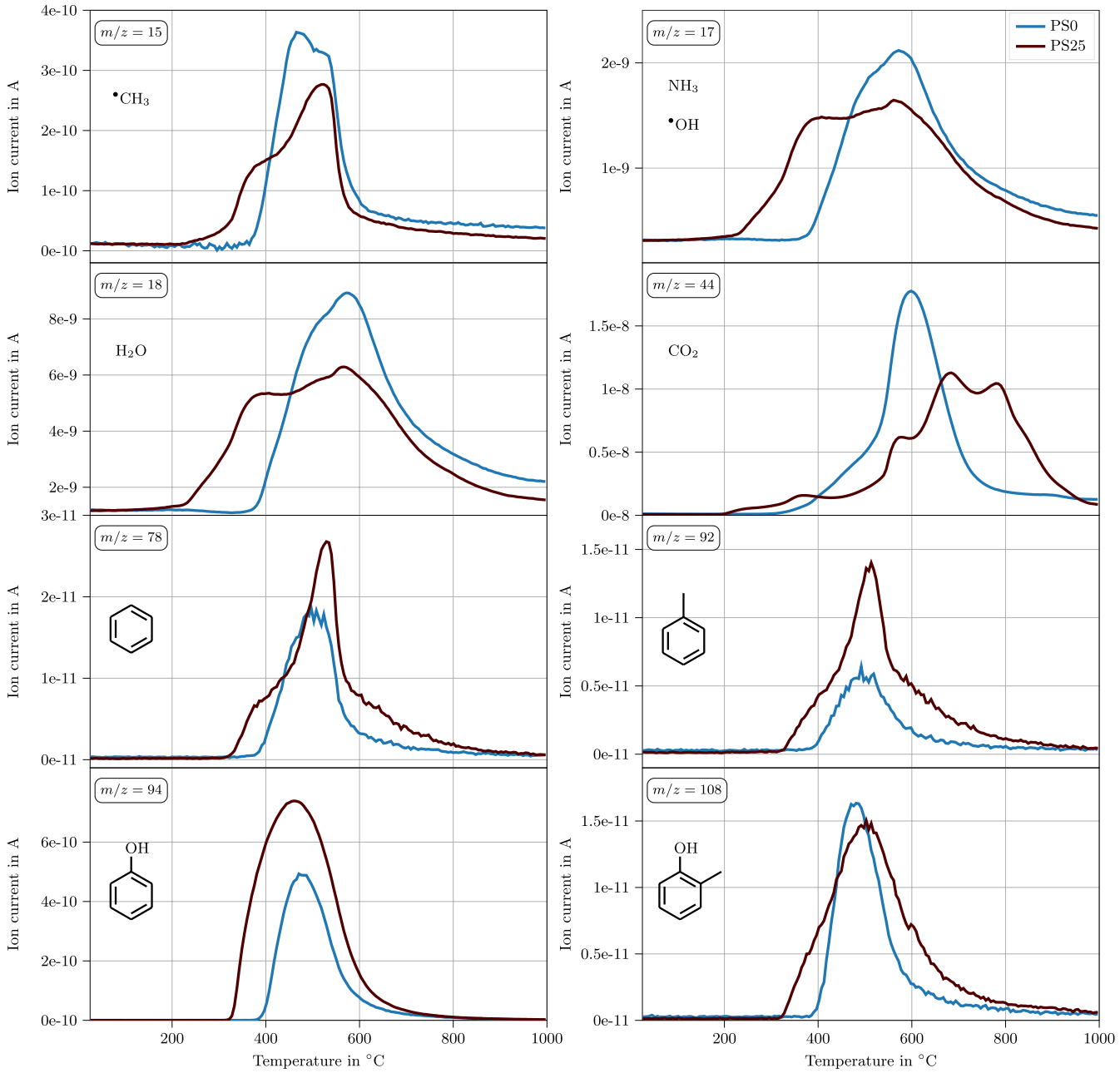

FIGURE 8 | The TG-MS data of PS0 and PS25 under synthetic air. [Color figure can be viewed at wileyonlinelibrary.com]

agent for the intumescent layer [65, 66]. After 8 min, the flame gradually extinguishes. PS25 loses about 58.5% of its mass, which is significantly lower than the 90.6% mass loss observed for PS0. Consequently, the THR and TSR of PS25 are reduced to 43.7 MJ/m^2 and 1330 m^2/m^2, respectively. Furthermore, the MARHE reaches about 115 kW/m^2 which is only a third of that of PS0, signifying a significant improvement in flame retardancy.

Petrella plots are commonly used to provide a quick and intuitive overview of CC results, focusing on the THR plotted against the ratio of PHRR to TTI [67]. Materials that ignite quickly and release a large amount of heat in a short time span are positioned in the upper right corner of the plot, indicating higher danger in fire scenarios. Conversely, FR materials, which ignite slowly and release less heat overall, are positioned in the lower left corner. In the context of PS added to DGEBA-type thermosets, its incorporation decreases both THR and PHRR, generally shifting materials toward the lower left corner of the Petrella plot. However, the addition of PS also reduces TTI significantly. As PS content increases above 20%, the decrease in TTI cannot be fully offset by the reduction in PHRR. Therefore, PS25, for instance, might lie to the right of PS20 in the Petrella plot due to its lower TTI, despite its lower THR and PHRR compared to PS20. Using the Petrella plot as a metric, the optimal composition of PS in thermosets for high flame retardancy applications could be debated. PS20 or PS25 may be preferred depending on whether minimizing THR or maximizing the delay in ignition is prioritized (see Figure 11).

Naturally, the FRI of the neat thermoset is one and increases for the further addition of effective FR into the matrix material

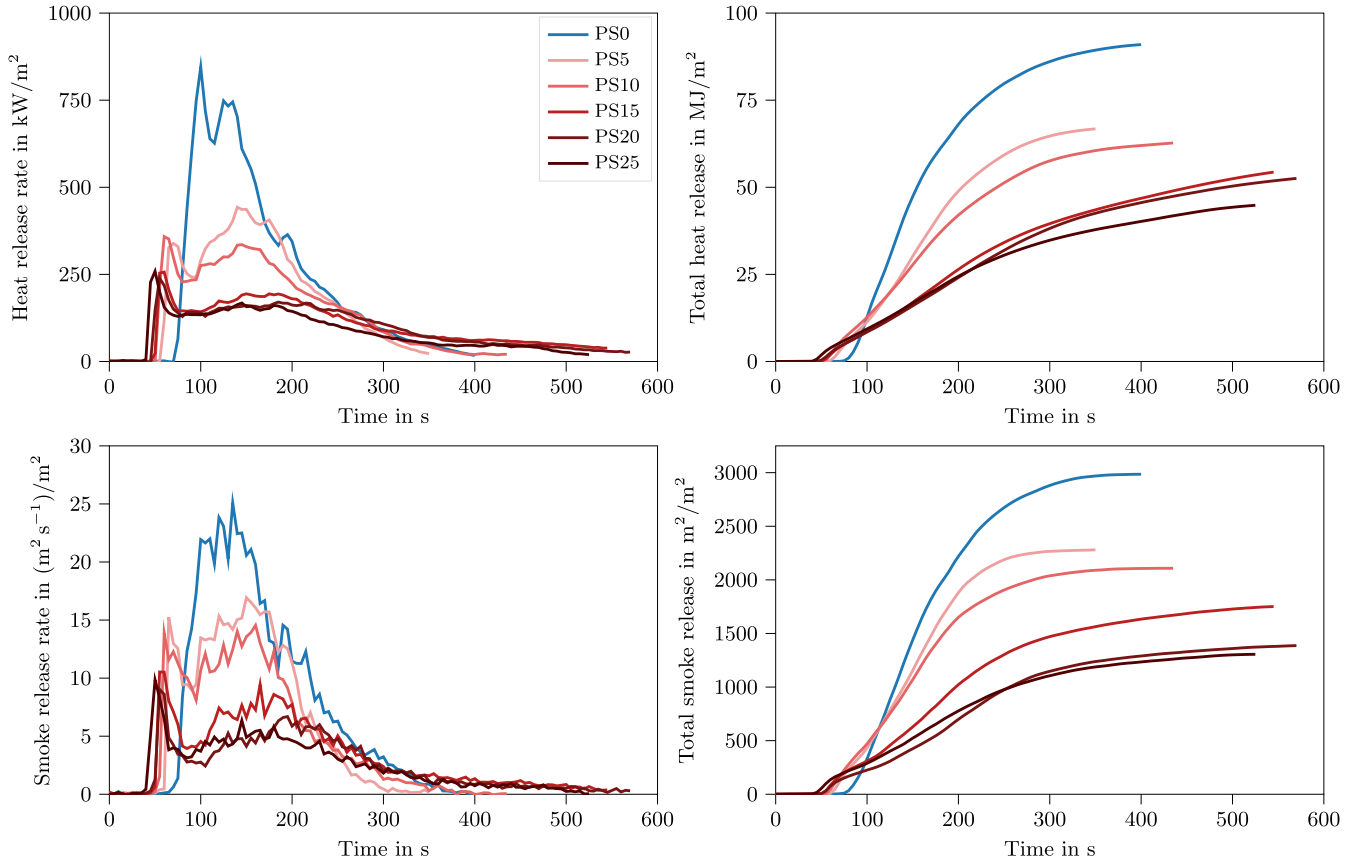

FIGURE 9 | Results of the CC of thermosets with different weight fractions of PS. Upper left: HRR. Upper right: THR. Lower left: SRR. Lower right: TSR. [Color figure can be viewed at wileyonlinelibrary.com]

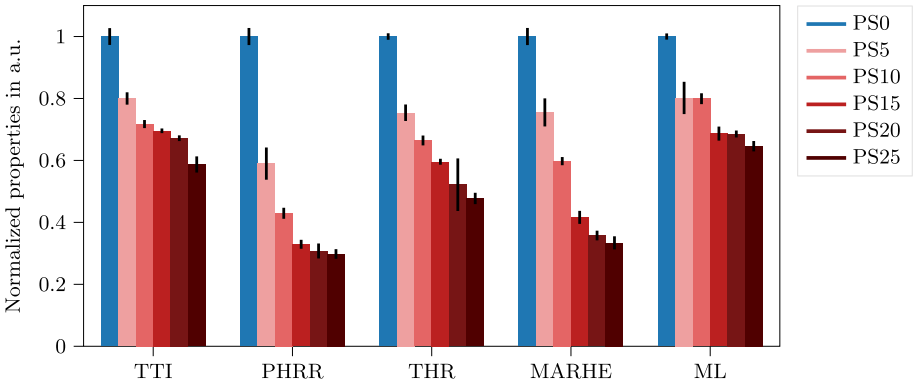

FIGURE 10 | Normalized key results of the CC of thermosets with different weight fractions of PS. [Color figure can be viewed at wileyonlinelibrary.com]

(see Table 2). For PS5, the FRI is approximately 1.8, indicating an improvement in flame retardancy compared to PS0. PS20 shows the highest FRI at around 4.18, suggesting it provides the most effective reduction in fire hazard among the formulations tested. PS25, while still effective, shows a slightly reduced FRI of 4.12 compared to PS20, likely due to a significant decrease in TTI relative to PHRR. Therefore, based on the FRI and considering the balance between reducing heat release and maintaining ignition resistance, PS20 appears to be the optimal weight fraction among those tested for enhancing flame retardancy in DGEBA cured with dicyandiamide. It achieves the highest FRI, indicating superior performance in reducing fire hazard compared to PS0 and other PS loadings. Still, the difference in FRI between PS20 and PS25 is minimal. According to the FRI regimes defined by Vahabi et al., the FR performance of PS20 and PS25 can be categorized as "good" ($1 < \text{FRI} < 10$) [30]. Still, the FRI only reflects the relative flame retardant effect that is achieved by the addition of the PS.

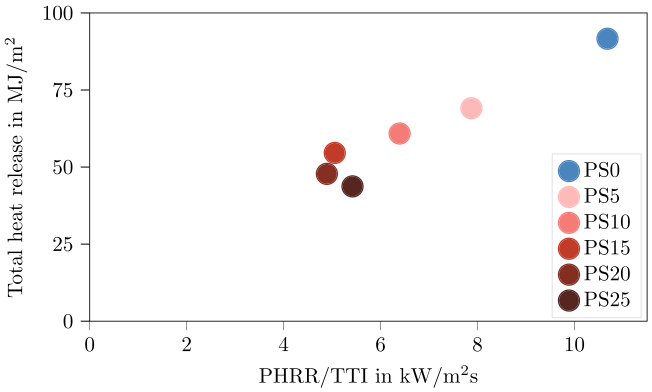

FIGURE 11 | Petrella plot of thermosets with different weight fractions of PS. [Color figure can be viewed at wileyonlinelibrary.com]

TABLE 2 | Gas and condensed phase modes of action with PS0 as reference, and FRI according to Equation (1) [35].

Label	Δ_{FIFD} in %	$\Delta_{Charring}$ in %	Δ_{PLE} in %	TPI in a.u.	FRI in a.u.
PS5	9.7	19.8	21.8	2.2	1.80
PS10	12.9	20.1	35.6	3.5	2.51
PS15	12.2	31.3	44.7	5.1	3.55
PS20	14.4	31.5	41.0	6.2	4.18
PS25	17.9	35.4	37.6	7.0	4.12

CC data is essential to measure the specific contributions of different modes of action to flame retardancy across samples. Analysis reveals that Δ_{FIFD} increases as the weight fraction of PS in thermosets rises (see Table 2). This trend likely stems from higher concentrations of flame-diluting compounds such as ammonia, water, and CO_2 in the flame zone, released during PS incineration. Previous studies have documented abundant production of these volatile flame-diluting agents during PS decomposition [22, 50]. Furthermore, $\Delta_{Charring}$ significantly increases with higher PS content in thermosets. Phosphate and ammonium phosphate groups induce dehydration within both PS and the thermoset matrix, promoting increased double bonds, enhanced cross-linking and aromatization of the material—a more thermally stable char [58]. This finding correlates well with the residual masses observed in TGA thermograms (see Figure 2). Similarly, Δ_{PLE} increases as PS weight fraction increases up to roughly 45% for PS15, indicating the protective effect of the intumescent layer. However, with further addition of PS into the thermosets, Δ_{PLE} begins to decrease. This is counter-intuitive since PS has been proven to be a powerful intumescent agent [19, 21]. In contrast, the TPI reflects the enhanced intumescence achieved through the incremental addition of PS into the thermoset matrix, with increasing values observed up to a weight fraction of 25%. Specifically, the TPI increases from 2.2 for PS5 to 7.0 for PS25, highlighting the usefulness of the TPI in assessing the influence of FRs on the reduction in the PHRR and THR.

After discussing the thermal decomposition mechanisms and fire behavior of DGEBA-type thermosets with different weight fractions of PS, it is essential to summarize the FR mechanisms of PS based on the observations made:

- Dilution of the flame zone: Ammonia, water, and CO_2 released during the GBC of PS contribute to the dilution of flammable gases and reduction of fuel efficiency [11, 68].
- Reduced mass loss: The phosphate and ammonium phosphate groups in PS cause dehydration, esterification, cross-linking, and aromatization of the condensed phase. Subsequently, less mass is pyrolyzed at a lower rate, resulting in a decreased heat of combustion [56–58].
- Protective barrier formation: Polyphosphate-based inorganic glasses act as insulators and protect the char [50, 61].
- Intumescent layer formation: The char formed might be expanded by the non-flammable gases and acts as a protective layer, shielding the underlying material from the heat of the flame [69].

These mechanisms collectively enhance the flame retardancy of the thermosets containing PS.

3.3 | Scanning Electron Microscopy

Figure 12 displays SEM images depicting the surface of CC specimens composed of PS25 after undergoing incineration. The surface exhibits a grainy texture attributed to embedded PS particles within the thermoset matrix. PS is prominently present on the surface, while the underlying matrix reveals a cellular structure (see Figure 12 bottom). During CC testing, the specimen expands, forming a dome-shaped structure. These observations collectively support the hypothesis that incorporating PS into the thermoset matrix facilitates the formation of an intumescent char layer, thereby enhancing the FR properties of PS.

4 | Conclusion and Outlook

This study investigates the FR performance of PS as a bio-based FR for DGEBA-type thermosets, marking its debut in polymeric bulk materials through a modified synthesis route. PS primarily enhances flame retardancy in the condensed phase by promoting increased charring and the formation of an intumescent layer. Additionally, the release of ammonia, water, and CO_2 contributes to flame dilution, as evident from CC data analysis.

Incorporating PS into the thermoset results in substantial reductions in PHRR, THR, and TSR with increasing weight fraction. Specifically, at 25% of PS, reductions of approximately 70%, 52%, and 53% are achieved for PHRR, THR, and TSR compared to PS0, respectively.

However, the acid catalyzed decomposition of both PS and the surrounding thermoset matrix notably decreases the $T_{5\%}$ and TTI. For PS weight fractions exceeding 20%, the reduction in TTI cannot be offset by an equivalent decrease in PHRR, resulting in a marginally inferior FR performance when assessed by Petrella plot and FRI. Depending on the application, 20% or 25%

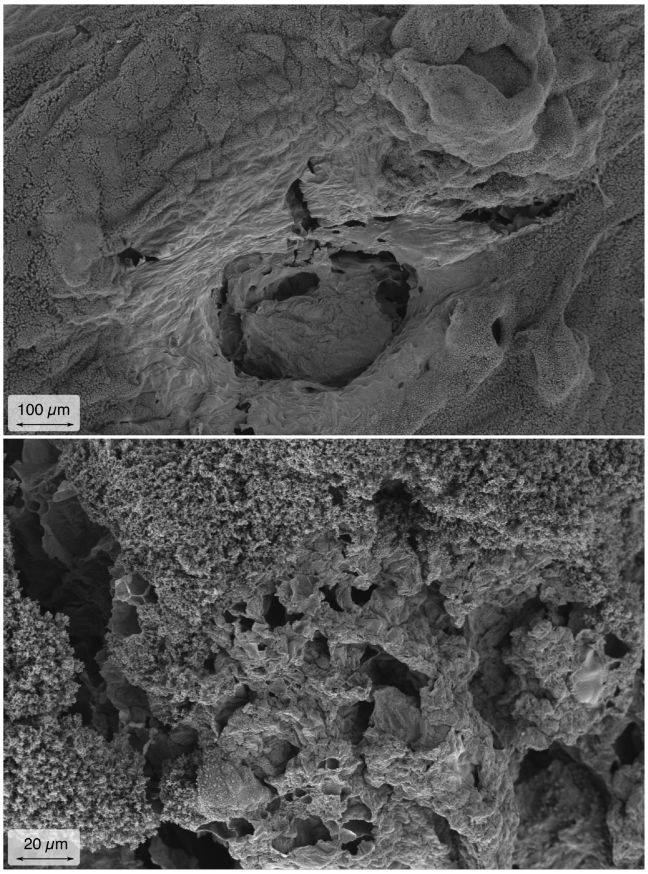

FIGURE 12 | SEM images of the surface of CC specimens made from PS25.

PS incorporation may be recommended as an FR for DGEBA cured with dicyandiamide.

Given the importance of synergistic effects in optimizing FR systems, the pioneering use of PS in polymers opens avenues for exploring optimal synergies with other compounds. As the global quest for sustainable and environmentally conscious fire safety solutions gains momentum, investigating PS as a bio-based FR represents a significant step toward a safer and more sustainable future.

Author Contributions

Florian Rothenhäusler: conceptualization (lead), investigation (equal), methodology (lead), supervision (lead), visualization (lead), writing – original draft (lead), writing – review and editing (lead). **Felix Ludik:** conceptualization (supporting), investigation (equal). **Lena Geiling:** investigation (equal). **Holger Ruckdaeschel:** funding acquisition (lead), project administration (lead), writing – review and editing (lead).

Acknowledgments

The authors want to thank Annika Pfaffenberger for her support during the experiments. We would like to thank Prof. Christina Roth of the Chair of Electrochemical Process Engineering for granting access to the TG-FTIR-MS analysis instrument. Open Access funding enabled and organized by Projekt DEAL. [Correction added on 2 March 2026, after first online publication: Projekt DEAL funding statement has been added]

Conflicts of Interest

The authors declare no conflicts of interest.

Data Availability Statement

The data that support the findings of this study are available from the corresponding author upon reasonable request.

References

1. A. K. Chaturvedi and D. C. Sanders, "Aircraft Fires, Smoke Toxicity, and Survival," *Aviation, Space, and Environmental Medicine* 67, no. 3 (1996): 275–278.

2. R. D. Peacock, R. W. Bukowski, W. J. Jones, P. A. Reneke, V. Babrauskas, and J. E. Brown, *Fire Safety of Passenger Trains* (U.S. Department of Transportation /Federal Railroad Administration, 1993).

3. Agency EMS, *Annual Overview of Marine Casualties and Incidents 2022* (European Maritime Safety Agency, 2022).

4. A. D. Blum, L. Birnbaum, R. Weber, et al., "Halogenated Flame Retardants in Consumer Products: Do the Fire Safety Benefits Justify the Health and Environmental Risks?," *Reviews on Environmental Health* 25 (2010): 261–305.

5. S. Kemmlein, D. Herzke, and R. J. Law, "Brominated Flame Retardants in the European Chemicals Policy of REACH—Regulation and Determination in Materials," *Journal of Chromatography A* 1216, no. 3 (2009): 320–333.

6. National Research Council (US) Subcommittee on Flame-Retardant Chemicals, *Toxicological Risks of Selected Flame-Retardant Chemicals* (National Academies Press (US), 2000).

7. J. Green, "A Review of Phosphorus-Containing Flame Retardants," *Journal of Fire Sciences* 10, no. 6 (1992): 470–487, https://doi.org/10.1177/073490419201000602.

8. M. M. Velencoso, A. Battig, J. C. Markwart, B. Schartel, and F. R. Wurm, "Molecular Firefighting—How Modern Phosphorus Chemistry Can Help Solve the Challenge of Flame Retardancy," *Angewandte Chemie International Edition* 57, no. 33 (2018): 10450–10467.

9. B. Schartel, "Phosphorus-Based Flame Retardancy Mechanisms—Old Hat or a Starting Point for Future Development?," *Materials* 3, no. 10 (2010): 4710–4745.

10. J. Hastie, "Molecular Basis of Flame Inhibition," *Journal of Research of the National Bureau of Standards Section A, Physics and Chemistry* 77, no. 6 (1973): 733.

11. K. Salmeia, J. Fage, S. Liang, and S. Gaan, "An Overview of Mode of Action and Analytical Methods for Evaluation of Gas Phase Activities of Flame Retardants," *Polymers* 3, no. 7 (2015): 504–526.

12. S. Huo, P. Song, B. Yu, et al., "Phosphorus-Containing Flame Retardant Epoxy Thermosets: Recent Advances and Future Perspectives," *Progress in Polymer Science* 114 (2021): 101366.

13. A. M. Sakharov, P. A. Sakharov, S. M. Lomakin, and G. E. Zaikov, "Novel Class of Eco-Flame Retardants Based on the Renewable Raw Materials," in *Polymer Green Flame Retardants*, ed. C. D. Papaspyrides and P. Kiliaris (Elsevier, 2014), 255–266.

14. L. Passauer, S. Fischer, H. Bender, S. Tech, and A. Wagenführ, "Use of Water-Soluble Nitrogen- and Phosphorus-Containing Polysaccharide Derivatives as Flame Retardants, Wood Composite Material With Improved Flame Retardance Properties and Process for Its Preparation," 2012, https://patents.google.com/patent/DE102012204238B4/en.

15. L. Passauer, S. Fischer, H. Bender, S. Tech, and A. Wagenführ, "Flame Retardants Comprising Polysaccharide Derivatives Containing Nitrogen and Phosphorus and Use Thereof to Improve the

Flame-Retardant Properties of Wood and Wood Composite Materials," 2013, https://patents.google.com/patent/EP2825615A1/en.

16. J. F. Robyt, *Starch: Structure, Properties, Chemistry, and Enzymology*, ed. B. O. Fraser-Reid, K. Tatsuta, and J. Thiem (Springer, 2008), 1437–1472, https://doi.org/10.1007/978-3-540-30429-6_35.

17. U. Heinze, D. Klemm, E. Unger, and F. Pieschel, "New Starch Phosphate Carbamides of High Swelling Ability: Synthesis and Characterization," *Starch-Stärke* 55, no. 2 (2003): 55–60.

18. L. Passauer and H. Bender, "Functional Group Analysis of Starches Reacted With Urea-Phosphoric Acid—Correlation of Wet Chemical Measures With FT Raman Spectroscopy," *Carbohydrate Polymers* 168 (2017): 356–364.

19. S. Gebke, K. Thümmler, R. Sonnier, S. Tech, A. Wagenführ, and S. Fischer, "Flame Retardancy of Wood Fiber Materials Using Phosphorus-Modified Wheat Starch," *Molecules* 25, no. 2 (2020): 335.

20. S. Gebke, K. Thümmler, R. Sonnier, S. Tech, A. Wagenführ, and S. Fischer, "Suitability and Modification of Different Renewable Materials as Feedstock for Sustainable Flame Retardants," *Molecules* 25, no. 21 (2020): 5122, https://www.mdpi.com/1420-3049/25/21/5122.

21. W. Ji, D. Wang, J. Guo, et al., "The Preparation of Starch Derivatives Reacted With Urea-Phosphoric Acid and Effects on Fire Performance of Expandable Polystyrene Foams," *Carbohydrate Polymers* 233 (2020): 115841.

22. F. Schäfer, "Investigations on the Influences of Paper Intrinsic Properties and Flame Retardants on Paper Materials Fire Properties," 2023 PhD Thesis, Technische Universität Darmstadt.

23. Y. Lu, P. Zhao, Y. Chen, et al., "A Bio-Based Macromolecular Phosphorus-Containing Active Cotton Flame Retardant Synthesized From Starch," *Carbohydrate Polymers* 298 (2022): 120076.

24. S. Azeroual, A. Belfkira, H. Wattati, M. Taourirte, and R. Jalal, "Obtaining and Microstructural Study of a Multifunctional Highly Phosphorylated Starch," *Starch-Stärke* 75, no. 11–12 (2023): 2300071.

25. G. Chen, Z. Liu, S. Deng, W. Zhao, and Q. J. Chen, "Application of Aminotrimethylphosphonic Acid Modified Starch-Based Flame Retardant in Cellulosic Paper," *Journal of Applied Polymer Science* 141 (2024): e56044.

26. F. Rothenhäusler, F. Ludik, R. Schneider, et al., "Influence of Post-Synthesis Heat Treatments on the Molecular Structure and Thermal Stability of Phosphatized Starch," *Macromolecular Chemistry and Physics* (2025): 2400252.

27. International Organization for Standardization, *ISO 5660-1:2015–03 (en); Reaction-to-Fire Tests—Heat Release, Smoke Production and Mass Loss Rate—Part 1: Heat Release Rate (Cone Calorimeter Method) and Smoke Production Rate (Dynamic Measurement)* (ISO, 2015).

28. B. Perret, B. Schartel, K. Stöß, et al., "Novel DOPO-Based Flame Retardants in High-Performance Carbon Fibre Epoxy Composites for Aviation," *European Polymer Journal* 47, no. 5 (2011): 1081–1089.

29. T. Neumeyer, G. Bonotto, J. Kraemer, V. Altstaedt, and M. Doering, "Fire Behaviour and Mechanical Properties of an Epoxy Hot-Melt Resin for Aircraft Interiors," *Composite Interfaces* 20, no. 6 (2013): 443–455.

30. H. Vahabi, B. K. Kandola, and M. R. Saeb, "Flame Retardancy Index for Thermoplastic Composites," *Polymers* 11, no. 3 (2019): 407.

31. H. Vahabi, E. Movahedifar, B. K. Kandola, and M. R. Saeb, "Flame Retardancy Index (FRI) for Polymer Materials Ranking," *Polymers* 15, no. 11 (2023): 2422.

32. E. Movahedifar, H. Vahabi, M. R. Saeb, and S. Thomas, "Flame Retardant Epoxy Composites on the Road of Innovation: An Analysis With Flame Retardancy Index for Future Development," *Molecules* 24, no. 21 (2019): 3964.

33. S. Brehme, B. Schartel, J. Goebbels, et al., "Phosphorus Polyester Versus Aluminium Phosphinate in Poly (Butylene Terephthalate) (PBT): Flame Retardancy Performance and Mechanisms," *Polymer Degradation and Stability* 96, no. 5 (2011): 875–884.

34. S. Rabe, Y. Chuenban, and B. Schartel, "Exploring the Modes of Action of Phosphorus-Based Flame Retardants in Polymeric Systems," *Materials* 10, no. 5 (2017): 455.

35. B. Schartel and K. Kebelmann, "Fire Testing for the Development of Flame Retardant Polymeric Materials," in *Flame Retardant Polymeric Materials: A Handbook*, 1st ed., ed. Y. Hu and X. Wang (CRC Press, 2019), 35–55.

36. M. Jauregui Rozo, S. Sunder, H. Ruckdäschel, and B. Schartel, "Char, Gas, and Action: Transfer of the Flame-Retardant Modes of Action in Epoxy Resins and Their Fiber-Reinforced Composites," *Polymer Testing* 140 (2024): 108610.

37. Z. Zhu, P. Lin, H. Wang, L. Wang, B. Yu, and F. Yang, "A Facile One-Step Synthesis of Highly Efficient Melamine Salt Reactive Flame Retardant for Epoxy Resin," *Journal of Materials Science* 55 (2020): 12836–12847.

38. H. Yu, X. Xu, Y. Xia, et al., "Synthesis of a Novel Modified Chitosan as an Intumescent Flame Retardant for Epoxy Resin," *E-Polymers* 20, no. 1 (2020): 303–316.

39. M. Shah, F. Jones, and M. Bader, "Residual Dicyandiamide (DICY) in Glass Fsssibre Composites," *Journal of Materials Science Letters* 4 (1985): 1181–1185.

40. J. B. Zhang, Z. C. Tan, S. H. Meng, S. H. Li, and L. M. Zhang, "Heat Capacity and Thermal Decomposition of Dicyandiamide," *Thermochimica Acta* 307, no. 1 (1997): 11–15.

41. W. T. Wang, S. H. Liu, Y. F. Cheng, Y. Wang, and C. F. Yu, "Evaluation of Thermal Decomposition Characteristics and Potential Hazards of 1-n-Butyl-3-Methylimidazolium Dicyanamide by STA, ARC, and TG-FTIR," *Journal of Thermal Analysis and Calorimetry* 147, no. 20 (2022): 11127–11137.

42. H. Cheng, H. Huang, Z. Liu, and J. Zhang, "Reaction Kinetics of CFRP Degradation in Supercritical Fluids," *Journal of Polymers and the Environment* 26 (2018): 2153–2165.

43. U. Braun, A. I. Balabanovich, B. Schartel, et al., "Influence of the Oxidation State of Phosphorus on the Decomposition and Fire Behaviour of Flame-Retarded Epoxy Resin Composites," *Polymer* 47, no. 26 (2006): 8495–8508.

44. R. Ullah, I. Ahmad, and Y. Zheng, "Fourier Transform Infrared Spectroscopy of "Bisphenol A"," *Journal of Spectroscopy* 2016, no. 1 (2016): 2073613.

45. Q. Hongqiang, W. Weihong, H. Jianwei, S. Jianhong, and X. Jianzhong, "Intumescent Flame Retardancy and Thermal Degradation of Epoxy Resin Filled With Ammonium Polyphosphate Using Thermogravimetric Analysis–Fourier Transform Infrared Spectroscopy and Thermogravimetric Analysis–Mass Spectrometry," *Journal of Macromolecular Science, Part B* 53, no. 2 (2014): 278–295.

46. C. G. Campbell, D. J. Astorga, E. Duemichen, and M. Celina, "Thermoset Materials Characterization by Thermal Desorption or Pyrolysis Based Gas Chromatography-Mass Spectrometry Methods," *Polymer Degradation and Stability* 174 (2020): 109032.

47. N. Shao, Y. Qu, L. Hou, et al., "Effect of Starch-Based Flame Retardant on the Thermal Degradation and Combustion Properties of Reconstituted Tobacco Sheet," *Cellulose* 28 (2021): 741–755.

48. S. A. Hedrick and S. S. Chuang, "Temperature Programmed Decomposition of Polypropylene: In Situ FTIR Coupled With Mass Spectroscopy Study," *Thermochimica Acta* 315, no. 2 (1998): 159–168.

49. X. Wang, Y. Hu, L. Song, W. Xing, and H. Lu, "Thermal Degradation Mechanism of Flame Retarded Epoxy Resins With a DOPO-Substitued

Organophosphorus Oligomer by TG-FTIR and DP-MS," *Journal of Analytical and Applied Pyrolysis* 92, no. 1 (2011): 164–170.

50. L. Passauer, "Thermal Characterization of Ammonium Starch Phosphate Carbamates for Potential Applications as Bio-Based Flame-Retardants," *Carbohydrate Polymers* 211 (2019): 69–74.

51. B. Kaur, I. S. Gur, and H. L. Bhatnagar, "Thermal Degradation Studies of Cellulose Phosphates and Cellulose Thiophosphates," *Die Angewandte Makromolekulare Chemie: Applied Macromolecular Chemistry and Physics* 147, no. 1 (1987): 157–183.

52. Y. Pan, Z. Luo, and B. Wang, "Cross-Linking Modification of Ammonium Polyphosphate via Ionic Exchange and Self-Assembly for Enhancing the Fire Safety Properties of Polypropylene," *Polymers* 12, no. 11 (2020): 2761.

53. H. J. de Jager and L. C. Prinsloo, "The Dehydration of Phosphates Monitored by DSC/TGA and In Situ Raman Spectroscopy," *Thermochimica Acta* 376, no. 2 (2001): 187–196.

54. B. Dittrich, K. A. Wartig, R. Mülhaupt, and B. Schartel, "Flame-Retardancy Properties of Intumescent Ammonium Poly (Phosphate) and Mineral Filler Magnesium Hydroxide in Combination With Graphene," *Polymers* 6, no. 11 (2014): 2875–2895.

55. G. Camino, L. Costa, and L. Trossarelli, "Study of the Mechanism of Intumescence in Fire Retardant Polymers: Part V—Mechanism of Formation of Gaseous Products in the Thermal Degradation of Ammonium Polyphosphate," *Polymer Degradation and Stability* 12, no. 3 (1985): 203–211.

56. J. E. Hendrix, J. E. Bostic, Jr., E. S. Olson, and R. H. Barker, "Pyrolysis and Combustion of Cellulose. I. Effects of Triphenyl Phosphate in the Presence of Nitrogenous Bases," *Journal of Applied Polymer Science* 14, no. 7 (1970): 1701–1723.

57. J. E. Hendrix, G. L. Drake, Jr., and R. H. Barker, "Pyrolysis and Combustion of Cellulose. III. Mechanistic Basis for the Synergism Involving Organic Phosphates and Nitrogenous Bases," *Journal of Applied Polymer Science* 16, no. 2 (1972): 257–274.

58. B. Schartel, B. Perret, B. Dittrich, et al., "Flame Retardancy of Polymers: The Role of Specific Reactions in the Condensed Phase," *Macromolecular Materials and Engineering* 301, no. 1 (2016): 9–35.

59. S. V. Levchik, G. Camino, M. P. Luda, L. Costa, G. Muller, and B. Costes, "Epoxy Resins Cured With Aminophenylmethylphosphine Oxide—II. Mechanism of Thermal Decomposition," *Polymer Degradation and Stability* 60, no. 1 (1998): 169–183.

60. P. Zheng, R. Wang, D. Wang, X. Peng, Y. Zhao, and Q. Liu, "A Phosphorus-Containing Hyperbranched Phthalocyanine Flame Retardant for Epoxy Resins," *Scientific Reports* 11, no. 1 (2021): 17731.

61. J. C. Markwart, A. Battig, L. Zimmermann, et al., "Systematically Controlled Decomposition Mechanism in Phosphorus Flame Retardants by Precise Molecular Architecture: P–O vs P–N," *ACS Applied Polymer Materials* 1, no. 5 (2019): 1118–1128.

62. S. Bourbigot, M. Le Bras, R. Delobel, R. Decressain, and J. P. Amoureux, "Synergistic Effect of Zeolite in an Intumescence Process: Study of the Carbonaceous Structures Using Solid-State NMR," *Journal of the Chemical Society, Faraday Transactions* 92, no. 1 (1996): 149–158.

63. M. Le Bras, S. Bourbigot, G. Camino, and R. Delobel, *Fire Retardancy of Polymers: The Use of Intumescence*, vol. 224 (Elsevier, 1998).

64. S. Bourbigot, M. Le Bras, S. Duquesne, and M. Rochery, "Recent Advances for Intumescent Polymers," *Macromolecular Materials and Engineering* 289, no. 6 (2004): 499–511.

65. M. Maqsood and G. Seide, "Investigation of the Flammability and Thermal Stability of Halogen-Free Intumescent System in Biopolymer Composites Containing Biobased Carbonization Agent and Mechanism of Their Char Formation," *Polymers* 11, no. 1 (2018): 48.

66. Q. Zhang, H. Liu, J. Guan, X. Yang, and B. Luo, "Synergistic Flame Retardancy of Phosphatized Sesbania Gum/Ammonium Polyphosphate on Polylactic Acid," *Molecules* 27, no. 15 (2022): 4748.

67. R. Petrella, "The Assessment of Full-Scale Fire Hazards From Cone Calorimeter Data," *Journal of Fire Sciences* 12, no. 1 (1994): 14–43.

68. S. Duquesne, M. Le Bras, S. Bourbigot, et al., "Analysis of Fire Gases Released From Polyurethane and Fire-Retarded Polyurethane Coatings," *Journal of Fire Sciences* 18, no. 6 (2000): 456–482.

69. G. Camino, L. Costa, and G. Martinasso, "Intumescent Fire-Retardant Systems," *Polymer Degradation and Stability* 23, no. 4 (1989): 359–376.